INSTITUTE OF PHYSICS PUBLISHING CLASSICAL AND QUANTUM GRAVITY

Class. Quantum Grav. **22** (2005) 723–735 doi:10.1088/0264-9381/22/4/006

Fast temporal evolution of a cosmic gravitational wave background spectrum

E Howell, D Coward, R Burman and D Blair

School of Physics, University of Western Australia (M013), Crawley WA 6009, Australia

Received 20 August 2004, in final form 14 December 2004
Published 1 February 2005
Online at stacks.iop.org/CQG/22/723

Abstract

We investigate the temporal evolution of a simulated gravitational wave spectrum modelled on a cosmological population of transient sources with characteristic rest-frame frequency of 1 kHz. Our purpose is to see what might be learned about the cosmic distribution of sources by the way in which such spectra build up over short spans of observation time. The spectral evolution depends on the history of source rate evolution and the observation time; and for a universal event rate of some tens s^{-1} (comparable to the neutron star birth rate) locked to the evolving star formation rate, the spectrum evolves rapidly within the first seconds of observation. A rapid increase in bandwidth occurs because of the large population of sources at moderate to high redshift. Spectra calculated using two observation-based star formation rate models and one simulated model show a relatively stationary low-frequency peak arising from the high-z sources and a time-dependent higher-frequency edge resulting from rarer nearby sources. The spectra converge to a stable form within an observation period of about 20 min for a universal event rate of about 15–30 s^{-1}. As a supplement, we provide Web-based movie files that highlight the rapid spectral evolution.

PACS numbers: 04.30.Db, 04.80.Nn, 97.60.Jd, 98.70.Vc, 98.80.−k

M This article features online multimedia enhancements

1. Introduction

Three long-baseline laser interferometric gravitational wave (GW) detectors have been built, or are near completion. The US Laser Interferometer Gravitational-Wave Observatory (LIGO) has completed several science runs; it consists of two 4 km arm detectors situated at Hanford, Washington, and Livingston, Louisiana. The Italian/French VIRGO Collaboration is completing a 3 km baseline instrument at Cascina, near Pisa[1]. These instruments are unlikely to be sensitive enough to detect many of the proposed astrophysical GW sources over practical observation times; but the next generation of interferometric detectors, planned to go online late this decade, should be sensitive to a host of sources. These 'advanced' interferometers could revolutionize our understanding of the universe, providing a new window to the cosmos not accessible by conventional astronomy.

The strongest GW sources, in the band most sensitive to advanced interferometers, include coalescing compact binaries (Flanagan and Hughes 1998, Miller *et al* 2004), core-collapse supernovae (Kotake *et al* 2004, Fryer *et al* 2004) and dynamic instabilities of post-collapse compact remnants (Fryer *et al* 2002). Transient GW emissions, associated with core-collapse supernovae (SNe), must occur frequently throughout the universe, and their combined signal will form a stochastic GW background, potentially detectable by advanced interferometric detectors.

Despite the uncertainty in the neutron star (NS) formation rate and in the GW emissions resulting from core-collapse SNe, estimates of the spectral properties of a stochastic GW background from such sources have been presented by a number of authors. Ferrari, Matarrese and Schneider (1999) calculated the stochastic background from a cosmological population of young, hot, rapidly rotating NSs that radiate GW energy through the r-mode instability. Coward, Burman and Blair (2001) investigated the GW background from NS birth by employing a representative sample of axisymmetric rotational core-collapse models developed by Zwerger and Müller (1997). Using the Einstein–de Sitter cosmology and a star formation rate (SFR) model from Madau, Pozetti and Dickenson (1998), they calculated the GW spectrum from sources in the range 0–5 of redshift z by convolving the differential rate of NS formation with a single-source GW fluence (time-integrated flux), integrated over z. They showed that the background spectrum retained a dependence on the single-source emission spectrum, and calculated a duty cycle of order unity. Howell *et al* (2004a) updated this work using simulated core-collapse GW waveforms, modelled with general relativity by Dimmelmeier, Font and Müller (2002, hereafter DFM). They found that the GW background from NS formation is unlikely to be detected by advanced LIGO detectors. However, preliminary results (Howell *et al* 2004b) show that the background will be considerably enhanced by dynamic post-collapse instabilities (bar modes) if they are a frequent feature of NS birth.

Coward, Burman and Blair (2002, hereafter CBB) developed a procedure for simulating the GW background from NS formation over cosmological distances. Assuming the SFR model of Madau, Della Valle and Panagia (1998) and the Einstein–de Sitter cosmology, they derived the probability density function for NS births as a function of z. They found the background GW strain to be dominated by sources at $z \approx 2$–3 and that the distribution of GW amplitudes is highly skewed, with skewness related to the low-z distribution of sources.

The purpose of this paper is to begin the study of the *time evolution* of such spectra. How does a spectrum build up over short spans of observation time before it settles down to a stationary pattern? And what can potentially be learned from short data spans about the cosmic distribution of the sources?

In this initial study, we extend the CBB simulation procedure to investigate the temporal evolution of a simulated GW spectrum, using three different source rate evolution models; these are based on a simulated SFR history that peaks at $z = 5$–6 and two observation-based SFR models, peaking at $z = 1$–2. We use a short duration, nearly monochromatic waveform, with a characteristic frequency of 1 kHz, allowing us to investigate the temporal

[1] For further information on these projects visit LIGO—http://www.ligo.caltech.edu and VIRGO—http://www.virgo.infn.it.

evolution of the spectra without the added complications arising from using more complex waveforms.

The paper is organized as follows: in section 2 we discuss the evolution of the NS birth rate throughout the Universe using the three different SFR models. We describe the simulation procedure in section 3 and present our resulting stationary and time-evolving spectra in section 4. In section 5 we discuss the main features of our results.

2. Neutron star birth rate evolution

The progenitors of NSs are relatively short-lived stars with masses greater than 8–10 $M_\odot$ and lifetimes of the order of tens of Myr; hence their formation rate will closely track the SFR (Yungelson and Livio 2000). But uncertainties in determining the SFR history from co-moving luminosity densities—particularly the allowance to be made for dust extinction (Porciani and Madau 2001)—have led to several alternative models for the cosmic SFR history being proposed. Here, we incorporate the uncertainty in SFR evolution by examining the effect of three proposed SFR models, two observation based and one a simulation.

Springel and Hernquist (2003, hereafter SH) conducted hydrodynamic simulations in a 'flat-Λ' cosmology (a spatially flat cosmology with a cosmological constant), within the 'cold dark matter' scenario, to study star formation from $z \approx 20$ to the present. In addition to gravitation and ordinary hydrodynamics, their work included the effects of star formation feedback processes (via SNe and stellar winds) on the interstellar medium. Their model shows a peak at $z \approx 5$–6, significantly higher than in the two observation-based models. It is supported by data from the Wilkinson Microwave Anisotropy Probe (Bennett *et al* 2003) that suggests that reionization occurred at $z > 10$ (Bunker *et al* 2004). Because of the uncertainty in the SFR at high z, we adopt the SH model to highlight the effect of high-z SFR evolution on the spectral evolution of a stochastic background of GWs, when compared with spectra obtained using two observation-based models peaking at $z = 1$–2.

We use an analytical fit to the SH simulation developed by Hernquist and Springel (2003), which includes a scaling related to the evolving expansion rate of the Universe, represented by the Hubble parameter:

$$h(z) \equiv H(z)/H_0 = [\Omega_\mathrm{m}(1+z)^3 + \Omega_\Lambda]^{1/2} \tag{1}$$

for a flat-Λ cosmology ($\Omega_\mathrm{m} + \Omega_\Lambda = 1$). We use $\Omega_\mathrm{m} = 0.3$ and $\Omega_\Lambda = 0.7$ for the $z = 0$ density parameters, and take $H_0 = 70$ km s^{-1} Mpc^{-1} for the Hubble parameter at the present epoch. With $\dot{\rho}_*$ denoting the mass converted to stars per unit time and volume, the fit takes the form

$$e(z) = \frac{\dot{\rho}_*[h(z)]}{\dot{\rho}_{*[z=0]}} = \frac{h^{4/3}}{1 + \alpha(h^{2/3} - 1)^3 \exp(\beta h^{7/6})}, \tag{2}$$

with $\dot{\rho}_{*[z=0]} = 0.013$ $M_\odot$ yr^{-1} Mpc^{-3}, $\alpha = 0.012$ and $\beta = 0.041$; we employ the fit in the form of a source rate evolution factor, $e(z)$, normalized to unity in our local intergalactic neighbourhood: $e(0) = 1$. Hernquist and Springel (2003, section 3) gave physical arguments for the general form of this function as an approximate fitting function. The SFR density rises exponentially from high z, reflecting the gravity-driven growth of dark-matter haloes. It reaches a peak at $z \approx 5$–6 and declines to $z = 0$ as $h^{4/3}(z)$, in proportion to the cooling rate of the haloes.

One can express the differential NS formation rate as the event rate in the redshift shell z to $z + \mathrm{d}z$ by the formula:

$$\mathrm{d}R = \frac{\mathrm{d}V}{\mathrm{d}z}\frac{r_0 e(z)}{1+z}\,\mathrm{d}z, \tag{3}$$

where dV is the cosmology-dependent co-moving volume element and $R(z)$ is the all-sky (4π solid angle) event rate, as observed in our local frame, for sources out to redshift z. Source rate density evolution is accounted for by the dimensionless evolution factor $e(z)$; as this is normalized to unity in the present-epoch universe ($z = 0$), r_0 is the $z = 0$ formation rate density, which we take as 5×10^{-12} NS s^{-1} Mpc^{-3} (Howell *et al* 2004a, section 2) . The $(1 + z)$ factor accounts for the time dilation of the observed rate by cosmic expansion, converting a source-count equation to an event rate equation.

Cosmological volume elements can be obtained from $H(z)$ by first calculating the luminosity distance from (cf Peebles 1993, p 332)

$$d_{\mathrm{L}}(z) = (1+z)\frac{c}{H_0}\int_0^z \frac{\mathrm{d}z'}{h(z')} \tag{4}$$

and using (e.g. Porciani and Madau 2001, equation (3))

$$\frac{\mathrm{d}V}{\mathrm{d}z} = \frac{4\pi c}{H_0}\frac{d_{\mathrm{L}}^2(z)}{(1+z)^2 h(z)}. \tag{5}$$

The cumulative NS birth rate, $R(z)$, as potentially observed by us, is calculated by integrating the differential rate from the present epoch to redshift z. It depends on cosmology through the factors $\mathrm{d}V/\mathrm{d}z$ and $e(z)$ in equation (3) for $\mathrm{d}R$. Integrating throughout the cosmos yields the Universal rate, R^{U}, of NS births as seen in our frame. For the SH model, Howell *et al* (2004a, section 2) calculated R^{U} to be about 25 s^{-1} for sources in $z = 0$–10; these events are separated temporally by a mean interval $\tau = 1/R^{\mathrm{U}} = 40$ ms.

For comparison with the SH model, we use two observation-based SFR models, the model SF1 of Porciani and Madau (2001), based on the work of Madau and Pozzetti (2000), and the model of Rowan-Robinson (2001), labelled as RR. Both models peak at a much lower z than does the SH model.

Model SF1 is based on observed rest-frame ultraviolet luminosity densities of the galaxy population as a whole. It can be expressed as an evolution factor of the form:

$$e(z) = \frac{(1+W)\,\mathrm{e}^{Qz}}{\mathrm{e}^{Rz} + W}. \tag{6}$$

Using the Einstein–de Sitter cosmology, Madau and Pozzetti (2000) found that $Q = 3.4$, $R = 3.8$ and $W = 45$ gave a reasonably good fit to ultraviolet continuum and $H\alpha$ luminosity densities from $z = 0$ to 4 after applying a moderate extinction correction of 1.2 mag at 150 nm and 0.55 mag at 280 nm. This SFR density increases rapidly from $z = 0$ to $z = 1$, peaks between $z = 1$ and 2 and gently declines at higher z.

The RR model was established on the basis that SFR evolution manifests itself as pure luminosity evolution, with the model parameters constrained by source counts and background radiation intensity measurements at sub-millimetre, far-infrared and mid-infrared wavelengths. It was developed further by King and Rowan-Robinson (2003) to improve the fit to near-infrared and optical data.

In the Einstein–de Sitter cosmology, model RR expressed as an evolution factor takes the form (King and Rowan-Robinson 2003):

$$e(z) = (1+z)^{-3P/2}\exp\{Q[1-(1+z)^{-3/2}]\}, \tag{7}$$

with P and Q positive parameters. It peaks at $1 + z = (Q/P)^{2/3}$. The power-law factor describes the increasing SFR density in the young Universe; the exponential factor describes its rapid decline towards our own epoch. The increase, with steepness measured by P, is interpreted as due to mergers of fragments as they are incorporated into galaxies. The decline, on a redshift scale of $2/(3Q)$ or time scale of $1/(H_0Q)$, is interpreted as due to exhaustion

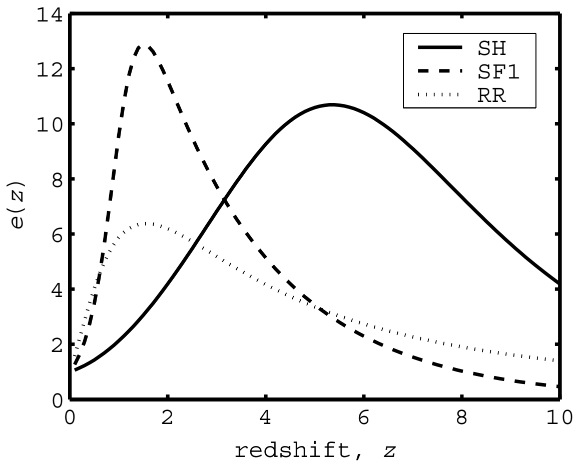

Figure 1. The dimensionless SFR density evolution factors $e(z)$, based on the SFR models SH (Springle and Hernquist 2003), SF1 (Porciani and Madau 2001) and RR (Rowan-Robinson 2001) all in the flat-Λ (0.3, 0.7) cosmology.

of gas available for star formation (itself the outcome of competition between gas loss to star formation and its return to the interstellar medium via SNe and stellar winds), together with the declining rate of galaxy interactions and mergers. Fitting yielded $P = 1.2$ and $Q = 5.4$.

Observation-based SFR models can be re-scaled to other cosmologies, as shown in the appendix of Porciani and Madau (2001). The observed luminosity density, and hence an observation-based SFR density, are proportional to $d_L^2 \big/ (\mathrm{d}V/\mathrm{d}z)$, which is proportional to $(1+z)^2 H(z)$, and so both scale as $H(z)$ among different cosmologies. But $e(z)$, which is normalized to unity at $z = 0$, just follows the shape of the SFR density curve and so scales as $h(z)$; that is, $e(z)/h(z)$ is invariant under change of cosmology. For converting the above evolution factors, equations (7) and (6), to a flat-Λ cosmology with $\Omega_m = 0.3$ and $\Omega_\Lambda = 0.7$, the scaling factor is

$$[0.3(1+z)^3 + 0.7]^{1/2}(1+z)^{-3/2}, \tag{8}$$

as follows from equation (1) for $h(z)$. The resulting $e(z)$ functions for all three SFRs are shown in figure 1.

Inserting r_0 and $e(z)$ into equation (3), along with a cosmological volume element function $\mathrm{d}V(z)$, calculated from equations (4) and (5), yields the differential source event rate. This is plotted in figure 2 for the three SFR models, showing that the differential NS birthrates calculated from the two observation-based models peak at about $z \approx 1$–2, whereas that obtained for the SH model peaks near $z = 4$.

Integrating from 0 to z yields the corresponding cumulative rates, $R(z)$, shown in figure 3. The asymptotic values, R^{U}, are not very different for the three SFR models: 25, 26 and 18 s^{-1} for SH, SF1 and RR, respectively.

3. Simulating the GW spectrum

The GW emission from SN core collapse is highly uncertain. For example, earlier models (DFM) predicted that the maximum GW amplitude occurs at the time of core bounce; however, recent hydrodynamical simulations of Müller *et al* (2004) suggest that the dominant contribution to the GW emission is not produced by stellar core bounce, but by neutrino

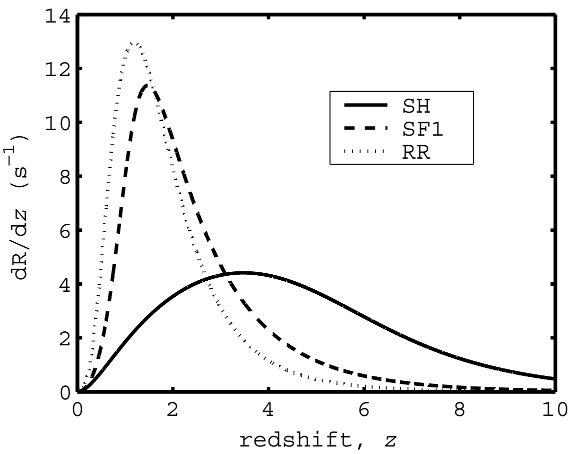

Figure 2. The differential rate of neutron star formation as a function of redshift, as potentially observed in our local frame, using the three SFR density evolution factors of figure 1.

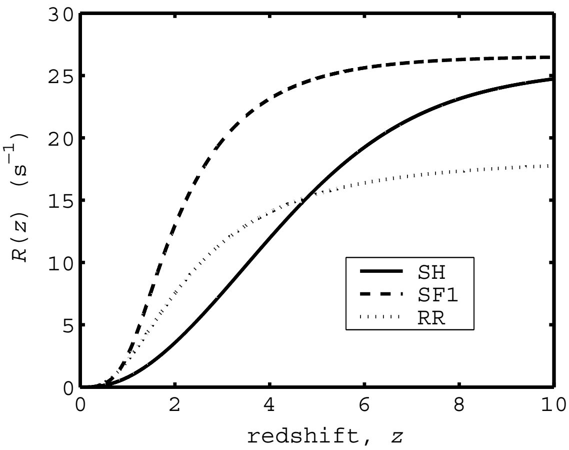

Figure 3. The cumulative NS formation rate as a function of z, as observed in our local frame, using the three SFR models. The asymptotic values show that the universal event rates, integrated throughout the cosmos, are 25 s^{-1} for SH, 26 for SF1 and 18 for RR.

convection behind the SN shock—this results in GW amplitudes an order of magnitude larger at about 100 ms after the core bounce.

For illustrative purposes, we use here a highly simplified input waveform, $h(t)$—a quasi-monochromatic damped sinusoid of characteristic rest-frame frequency 1 kHz and duration 10 ms, with a maximum dimensionless strain amplitude of 7×10^{-24} at a fiducial distance of 10 Mpc. The waveform duration is approximately that of strongest GW emission of a DFM type I (regular collapse) waveform, corresponding roughly to the ringdown phase.

The received amplitude and duration of the waveform are defined by the random variable z, generated from a probability density function $P(z)$, obtained by normalizing $\mathrm{d}R/\mathrm{d}z$ by the universal rate, integrated throughout the cosmos, as seen in our frame (cf CBB, section 3):

$$P(z)\,\mathrm{d}z = \mathrm{d}R/R^{\mathrm{U}}; \tag{9}$$

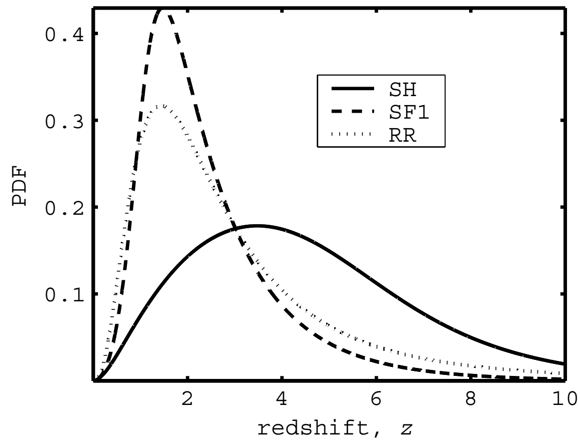

Figure 4. The probability density function for NS births as a function of redshift, using the three SFR density evolution factors of figure 1.

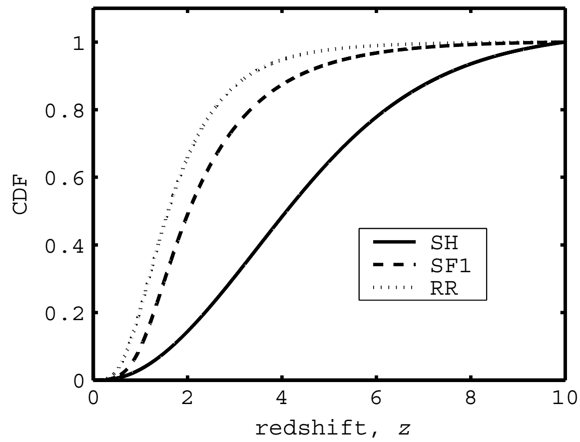

Figure 5. The cumulative distribution function for NS births as a function of redshift, using the three SFR models. We see a greater probability of events occurring at low redshift for the observation-based models, SF1 and RR, than for the simulated model SH.

this defines $P(z)\,\mathrm{d}z$ as the probability that an event occurred in the redshift shell z to $z + \mathrm{d}z$. Thus, normalizing the differential event rate $\mathrm{d}R(z)$ converts it to a probability distribution function with z treated as a random variable. Figure 4 plots $P(z)$, showing that most of the events occur at $z \approx 3$–4 for the SFR model SH and at $z \approx 1.5$–2 for the SF1 and RR models. The corresponding cumulative distribution function $C(z)$, giving the probability of an event occurring in the redshift range 0 to z, is the normalized cumulative rate:

$$C(z) = R(z)/R^{\mathrm{U}}, \tag{10}$$

which is shown in figure 5 for the three SFR models. This figure highlights the bias towards lower-z events for the observation-based models in comparison with the SH model. We use the inverse function of $C(z)$ to produce values of z by employing a random number generator to select values from $C(z)$.

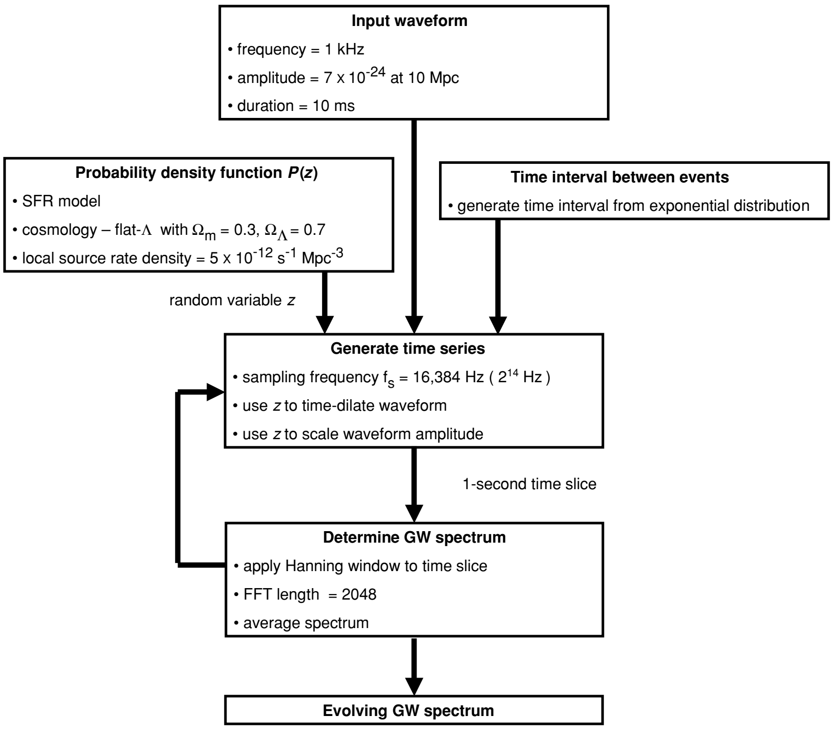

Figure 6. Flow chart outlining the simulation procedure for calculating the GW spectral evolution. To produce a time series, the standard input waveform is scaled in amplitude and time dilated according to the random variable z, obtained from the probability distribution shown in figure 4. As the events are independent, they form a Poisson-distributed time series, with the temporal separations between successive events following an exponential distribution.

For a simulation of N events, the GW amplitude for each $h_{\rm i}(t)$, $i = 1, \ldots, N$, is scaled inversely by the luminosity distance $d_{\rm L}(z)$ and the signal duration is time dilated by the factor $(1+z)$. As the temporal distribution of events in our frame is a stochastic, memory-less point process described by Poisson statistics, the time interval between successive events, τ, will follow an exponential distribution. Successive waveforms are generated and combined to form a wave train defined by the random variables z and τ. Because the signal durations are of order milliseconds, a high sampling rate of 16 384 Hz (2^{14} Hz) ensures that the sampled data stream is free from any discontinuities that would produce spurious high-frequency components in the spectrum.

Time slices, corresponding to 1 s of real-time data, are simulated and fast Fourier transforms (FFTs) of length 2048 are calculated using a Hanning window. Individual spectra, $S_{\rm n}(f)$ in Hz^{-1}, of these time slices are accumulated at a rate $\approx$4 times 'real' time for our 2.8 GHz processor. Successive spectra are averaged to yield a power spectrum defined as

$$S(f) = \sum_n S_{\rm n}(f)/n = |h(f)|^2, \tag{11}$$

where $h(f)$, in Hz$^{-1/2}$, is the GW background strain.

This procedure allows us to study the temporal evolution for different simulation lengths of data, corresponding to observations of different durations. A schematic of the procedure is presented as a flow diagram in figure 6.

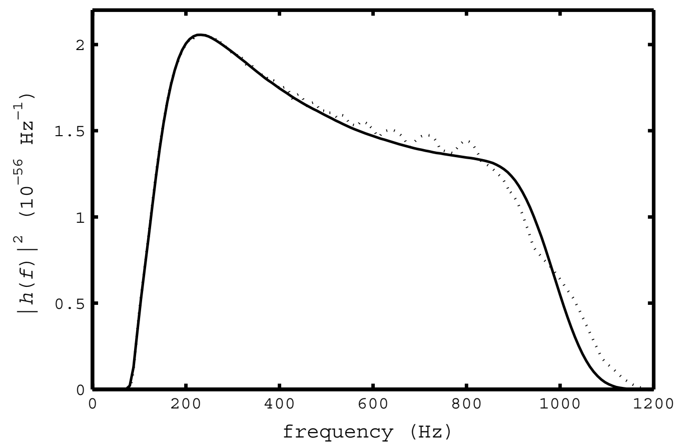

Figure 7. The power spectrum of the GW background as a function of observation frequency for 30 million simulated events using the SH SFR model, calculated by averaging FFTs of length 2048 (solid line). For comparison, the power spectrum obtained by a convolution of the single-source spectrum with the differential rate, integrated over redshift, is also shown (dotted line); this has been scaled to the maximum magnitude of the simulated spectrum. The oscillations are numerical noise. The peak at just beyond 200 Hz corresponds to the maximum of the differential rate of source formation (figure 2).

4. Results

4.1. Stationary spectra

Figure 7 shows the averaged GW power spectrum using the SH SFR for a simulation of 30 million events—equivalent to two weeks of data for an event rate of 25 s^{-1} in our frame. For comparison, this figure also shows a power spectrum calculated by convolving a simulated single-source GW spectrum with the differential rate of source formation over the redshift range $0.002 < z < 10$, where $z = 0.002$ corresponds to about 10 Mpc. The ripples in the convolved spectrum are numerical noise. The amplitude of the power spectrum $|h(f)|^2 \approx 10^{-56}$ Hz^{-1} is in correspondence with the background strain $h(f) \approx 10^{-28}$ $\mathrm{Hz}^{-1/2}$, calculated for a GW background resulting from NS birth using the waveforms of DFM (Howell *et al* 2004a).

The most prominent feature of the integrated spectrum is the broad peak at 200–250 Hz, resulting from the high rate of events in the redshift shell $4.0 > z > 3.5$, corresponding to the maximum of the differential event rate (figure 2). At frequencies greater than this there is a gently decreasing trend in power spectral density towards the rest-frame frequency of 1 kHz. The temporally simulated spectrum converges to the integrated convolved spectrum after about 8×10^5 events.

Figure 8 shows the averaged GW power spectrum obtained for a simulation of 5 million events for each of the observation-based SFR models SF1 and RR. As the simulated spectrum reaches equilibrium after only $\approx 10^5$ events, corresponding to a rate of 20–40 s^{-1}, we reduced our simulation time to compare these two spectra. Their most prominent features are the broad peaks at 450–550 Hz, resulting from the high rates of events in the redshift shell $1.0 < z < 1.5$. As for the simulations based on the SH model, the spectra peak at redshift corresponding to the maximum of the differential rate of events (figure 2). Because the more frequent events are at lower redshift in these models, the inverse-square luminosity distance dependence means that they exhibit a more rapidly decreasing trend in power spectral density from this maximum value towards the $z = 0$ events at rest-frame frequency.

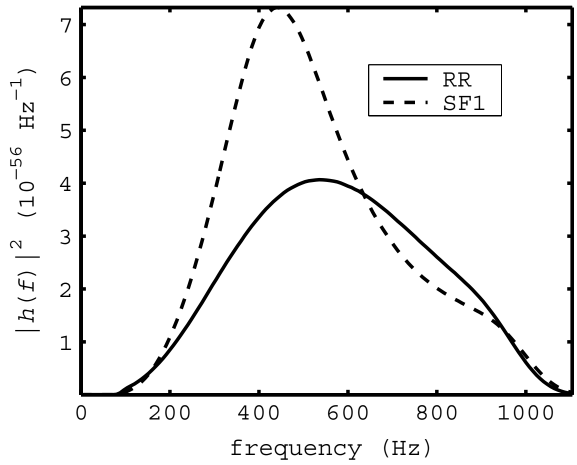

Figure 8. The power spectrum of the GW background as a function of observation frequency, simulated using the observation-based SFR models SF1 and RR. The spectra are calculated by averaging FFTs of length 2048 for 5 million simulated events. As evident in figure 7, the peak of each spectrum corresponds to the maximum of the differential rate of source formation (figure 2).

4.2. Spectral evolution

For the SH simulated spectrum, with a universal event rate of 25 s^{-1}, the fastest spectral evolution occurs during the first seconds of observation time. This characteristic is dramatically highlighted in the supplementary animation, where there is an initial rapid increase in bandwidth from 550 Hz to 900 Hz for the first events, corresponding to sources in $z \approx$ 9–0.7.

Figure 9 shows three frames from the movie at increasing times, along with the corresponding SF1 and RR simulated spectra. This figure illustrates the trend of increasing bandwidth as the number of events increases. With a universal event rate of about 26 s^{-1}, the SF1 spectrum displays a rapid increase of bandwidth from 650 Hz to 950 Hz for the first 10 s, corresponding to sources in $z \approx$ 9–0.05. The RR spectrum displays the slowest increase in bandwidth, from 600 Hz to 800 Hz for the same period, corresponding to sources in $z \approx$ 9–0.3. This slower bandwidth increase is a result of a smaller universal event rate of about 18 s^{-1} in this model.

After this initial rapid spectral evolution, there is an intermediate period corresponding to $N = 10^2$–10^4 events. For data streams with temporal durations corresponding to $N \approx$ 300–400, the rate of increase in bandwidth decreases because events outside the shell $0.2 < z < 0.9$ are less probable. The temporal evolution of the spectrum during this time is dominated by two components—a stable low-frequency peak at about 250 Hz, corresponding to the maximum of the differential source rate, and a non-stationary higher-frequency edge resulting from sources at $z < 0.2$. The latter component is dependent on the rate of low-z events, which manifest as time-dependent fluctuations in the higher-frequency edge, showing up because of the inverse-square luminosity distance dependence.

Also apparent during this intermediate period are smaller magnitude non-stationary peaks in the 400–700 Hz band as N increases—a result of the small sample space. As the spectrum continues to evolve we see a gradual broadening in bandwidth and smoothing of non-stationary features. The spectrum converges to a broad 200–700 Hz monotonically decreasing band from sources in the intermediate range 4–0.4 of z. For spectra with $N \gtrsim 10^5$, the high-frequency

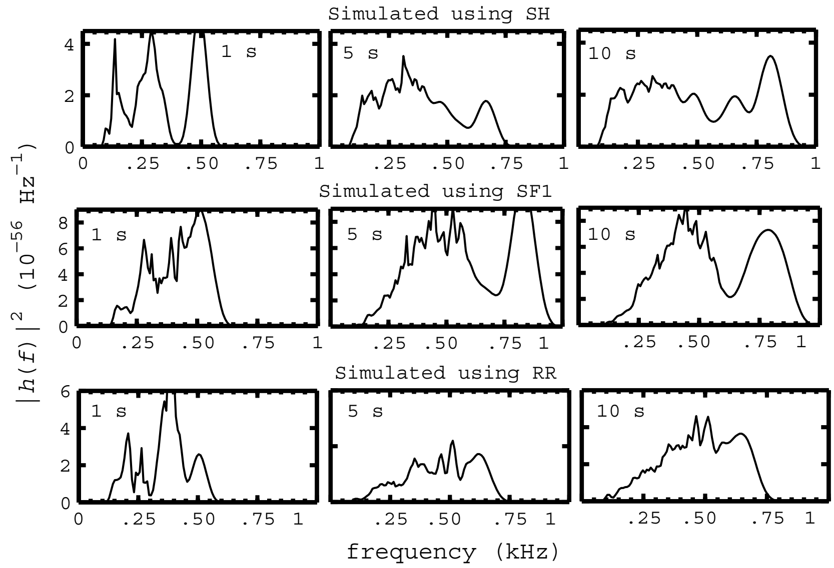

Figure 9. The initial rapid evolution of the GW power spectrum, simulated using the SH, SF1 and RR SFR models, for the first 10 s of observation time. All spectra show an initial bandwidth of about 450 Hz for the first second, equivalent to about 25 events for SH, 26 for SF1 and 18 for RR. The panels show increases in bandwidth toward higher frequencies over the next few seconds, a result of events occurring at lower redshifts. The RR spectrum shows the slowest increase, due to the lower event rate in this model.

edge is averaged out. For $N \gtrsim 10^7$, the spectrum converges to the limiting stationary spectral shape shown in figure 7.

Figure 10 shows that the non-stationary higher-frequency edge, apparent during the period corresponding to $N \approx$ 300–400 events in the SH simulated spectrum, is also evident in the SF1 and RR spectra. But this feature is most prominent in the SH spectrum, as a result of the larger fraction of high-z events, which weight the spectrum towards lower frequency.

5. Discussion

This study investigates the temporal evolution of a GW spectrum from a cosmological population of transient sources using a Monte Carlo simulation, and compares the spectra obtained using three proposed SFR models. Compared to the spectrum based on the SH SFR model, the two observation-based SFR models predict GW spectra that peak towards higher frequencies.

In studying the temporal evolution of the GW spectrum, we can observe how rarer events influence the bandwidth evolution. We find that the evolving bandwidth is dependent on the event rate and the distribution of events in redshift. For models with a similar redshift distribution, the rate of increase in bandwidth within the first seconds is dependent on the universal event rate.

In this initial study, we have employed a highly idealized quasi-monochromatic GW source waveform. We intend to use more realistic waveforms to investigate the dependence of the evolution of the spectrum on the choice of source model. Even with more realistic model waveforms, it is plausible that there are dominant frequencies for each waveform type that will characterize the temporally evolving spectrum.

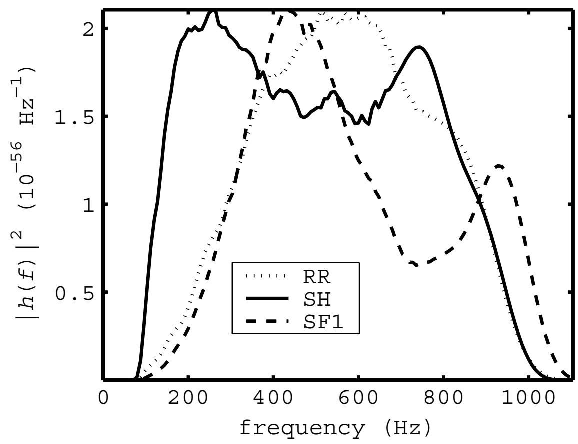

Figure 10. The power spectra for 10 000 events simulated using the SH, SF1 and RR source rate evolution models; they are scaled to the maximum value of the SH simulated spectrum for clarity. Noting the comparison with figure 7, we see that this intermediate period of temporal evolution, although non-stationary, can be characterized by a broad peak at low frequency, corresponding to the maximum of the differential rate, and a higher-frequency component resulting from events in the redshift range $z = 0.002$ to 0.2.

This study investigates the temporal evolution of the GW spectrum over short observation times relative to the much longer science data already available from LIGO. A more complete understanding of the spectral evolution over observation times of up to a year is important for optimizing detection algorithms for transient cosmological GW sources. Advanced GW interferometric detectors will most likely detect the rarer but stronger nearby sources, which manifest as the high-frequency edge (see figure 9) in our simulations. Cross-correlation is the optimum detection method for more frequent high-z events, but a Bayesian-based thresholding procedure utilizing a model for the source distribution may be optimal for the less frequent low-z events. We plan to extend this work to develop a comprehensive model for the bandwidth evolution and apply this model to parallel signal processing algorithms that encompass events at both high and low z.

Acknowledgments

This research is supported by the Australian Research Council Discovery grant DP0346344 and is part of the research programme of the Australian Consortium for Interferometric Gravitational Astronomy (ACIGA). David Coward is supported by an Australian Postdoctoral Fellowship. The authors thank the referee for making some constructive suggestions, which have led to a fuller paper incorporating a comparison of spectra based on different SFR models. We also thank Dr André B Fletcher (Shanghai Astronomical Observatory) for discussions and a careful reading of the manuscript.

References

Bennett C L *et al* 2003 *Astrophys. J. Suppl.* **148** 1
Bunker A J, Stanway E R, Ellis R S and McMahon R G 2004
Coward D, Burman R and Blair D 2001 *Mon. Not. R. Astron. Soc.* **324** 1015
Coward D, Burman R and Blair D 2002 *Mon. Not. R. Astron. Soc.* **329** 411

Dimmelmeier H, Font J and Müller E 2002 *Astron. Astrophys.* **393** 523
Ferrari V, Matarrese S and Schneider R 1999 *Mon. Not. R. Astron. Soc.* **303** 247
Flanagan É É and Hughes S A 1998 *Phys. Rev.* D **57** 4535
Fryer C L, Holz D E and Hughes S A 2002 *Astrophys. J.* **565** 430
Fryer C L, Holz D E and Hughes S A 2004 *Astrophys. J.* **609** 288
Hernquist L and Springel V 2003 *Mon. Not. R. Astron. Soc.* **341** 1253
Howell E, Coward D, Burman R, Blair D and Gilmore J 2004a *Mon. Not. R. Astron. Soc.* **351** 1237
Howell E, Coward D, Burman R, Blair D and Gilmore J 2004b *Class. Quantum Grav.* **21** S551
King A J and Rowan-Robinson M 2003 *Mon. Not. R. Astron. Soc.* **339** 260
Kotake K, Yamada S, Sato K, Sumiyoshi K, Ono H and Suzuki H 2004 *Phys. Rev.* D **69** 124004
Madau P, Della Valle M and Panagia N 1998 *Astrophys. J.* **297** L17
Madau P and Pozzetti L 2000 *Mon. Not. R. Astron. Soc.* **312** L9
Madau P, Pozzetti L and Dickenson A 1998 *Astrophys. J.* **498** 106
Miller M, Gressman P and Suen W-M 2004 *Phys. Rev.* D **69** 064026
Müller E, Rampp M, Buras R, Janka H-T and Shoemaker D H 2004 *Astrophys. J.* **603** 221
Peebles P J E 1993 *Principles of Physical Cosmology* (Princeton, NJ: Princeton University Press)
Porciani C and Madau P 2001 *Astrophys. J.* **548** 522
Rowan-Robinson M 2001 *Astrophys. J.* **549** 745
Springel V and Hernquist L 2003 *Mon. Not. R. Astron. Soc.* **339** 312
Yungelson L R and Livio M 2000 *Astrophys. J.* **528** 108
Zwerger T and Müller E 1997 *Astron. Astrophys.* **320** 209